Fault Diagnosis Based on Compressed Sensing of Multisource Data

Xianglong You (xianglongyou@cqu.edu.cn)
Chongqing University
Zhongwei Deng
Chongqing University
Kai Zhang
Chongqing University
Jiacheng Li
Chongqing University
Hang Yuan
Henan University of Technology

Research Article

Keywords: Compressed sensing, Sparse representation, Fault diagnosis, Information fusion

Posted Date: March 7th, 2022

DOI: https://doi.org/10.21203/rs.3.rs-1344545/v1

Title page

Fault Diagnosis Based on Compressed Sensing of Multisource Data

Xiang-long You, is currently a PhD candidate at *College of Mechanical and Vehicle Engineering, Chongqing University, China*. He received his Master degree on vehicle engineering from *Beijing Institute of Technology, China*, in 2017. His research interests include fault diagnosis of mechanical systems and power battery systems.
Tel: +86-15937176261; E-mail: xianglongyou@cqu.edu.cn

Zhong-wei Deng, is currently a post doc at *College of Mechanical and Vehicle Engineering, Chongqing University, China.* He received his Ph.D. degree from *Shanghai Jiaotong University, China*, in 2019. His research interests include data-driven and electrochemical mechanism modeling, parameter identification, states estimation, health diagnosis, and cascade utilization of lithium-ion batteries.
E-mail: dengzhongw@cqu.edu.cn

Kai Zhang, is currently a PhD candidate at *College of Automotive Engineering, Chongqing University, China*. His research interests include the fault diagnosis of batteries, sensors, and actuators in lithium-ion battery systems.
E-mail: kaizhang@cqu.edu.cn

Jia-cheng Li, is currently an Engineer at *College of Mechanical and Vehicle Engineering*, *Chongqing University*. His research focuses on hybrid electric vehicles (HEVs), and modeling and thermal management of lithium-ion batteries. He received the B.E. degree in power engineering and the M.S. degree in vehicle engineering from *Chongqing University, Chongqing, China*, in 2014 and 2016, respectively.
E-mail: lijiacheng91@foxmail.com

Hang Yuan, is currently a lecturer at *Henan University of Technology, China*. He received his PhD degree from *Beihang Universtiy, China*, in 2016. His research interests include prognostics and health management, industrial data mining.
E-mail: hangyuan@haut.edu.cn

Corresponding author：Jia-cheng Li　E-mail：lijiacheng91@foxmail.com

ORIGINAL ARTICLE

Fault Diagnosis Based on Compressed Sensing of Multisource Data

Xiang-Long You[1,2] • Zhong-Wei Deng[1,2] • Kai Zhang[1,2] • Jia-Cheng Li [1,2*] • Hang Yuan[3]

Received June xx, 202x; revised February xx, 202x; accepted March xx, 202x

Abstract: With the development of the internet of things (IoT) and the application of 5G communication, fault diagnosis of massive multisource sensor data becomes more and more important. In this study, a compressed multisource sensor data-based fault diagnosis scheme is proposed, and its advantages include high data compression and fusion efficiency, low computational cost, and a fast online training sample updating rate. The method includes reference matrix construction, reference matrix compression and fusion, sparse vectors calculation, testing sample reconstruction, and quality evaluation. First, a reference matrix is constructed with labeled multisource sensor data, and each column in the matrix is composed of data samples collected from different sources. Then, the reference matrix is compressed using a measurement matrix, meanwhile, the multisource data samples are fused based on weighted summation during the compression. Later, sparse representation based on batch matching pursuit algorithm is conducted, in this step, the compressed testing sample is represented by the compressed reference matrix, and the output of the sparse representation is a sparse vector. After that, elements in the sparse vector corresponding to different patterns are retained exclusively while other elements are set to zero, respectively, and estimated testing samples are reconstructed with the compressed reference matrix and the processed sparse vector. Finally, based on reconstruction quality evaluation, the pattern of the testing sample is determined. Two cases are employed to validate the effectiveness of the proposed approach, including landfill gas power generator maintenance pattern recognition and multiple redundancy aileron actuator fault diagnosis, and the detection accuracy is 96.13% and 96.67%, respectively.

✉ Jia-cheng Li
lijiacheng91@foxmail.com

[1] College of Mechanical and Vehicle Engineering, Chongqing University, Chongqing 400044, China

[2] State Key Laboratory of Mechanical Transmissions, Chongqing University, Chongqing 400044, China

[3] School of Electrical Engineering, Henan University of Technology, Zhengzhou 450001, China

Keywords: Compressed sensing • Sparse representation • Fault diagnosis • Information fusion

1 Introduction

Fault diagnosis is a key technique of Prognostics and Health Management (PHM). With the application of the internet of things (IoT) and the application of 5G communication infrastructure, multisource sensor data becomes a key component of fault diagnosis[1, 2]. The increasing data provides useful information for fault diagnosis[1, 3]. However, fault diagnosis based on massive multisource data faces several challenges, such as multisource sensor data fusion, massive data compression for real-time fault diagnosis, and online training sample updating and re-training for variable working conditions[4].

To fuse the collected data from multiple sensors efficiently, a variety of fusion models have been proposed[5]. Conventional data fusion-based fault diagnosis methods for multisource sensor data include some simple processing algorithms, fuzzy logic algorithms[6], probability-based algorithms, and artificial intelligence algorithms[7-9], etc. For example, one of the simple processing algorithms is the weighted average method. Fuzzy logic algorithms for fault diagnosis include fuzzy clustering algorithms, fuzzy logic reasoning, and a combination of other algorithms. Probability-based algorithms include those based on D-S evidence theory and Bayesian theory[10], etc. Although these fusion models are widely used for fault diagnosis, several challenges are faced in practical applications, such as determining weights in the weighted average method or determining parameters in artificial intelligence algorithms. Thus, an ideal multisource sensor data fusion method should retain as much useful information as possible, and the weights or parameters are easy to determine or not required.

To reduce the computational cost of fault diagnosis with large amount of data, dimensionality reduction methods are

essential. Dimensionality reduction methods mainly include feature extraction and feature selection. Feature extraction refers to extracting a new and smaller representation set from the original dimension space, these algorithms can be divided into linear and nonlinear techniques, representative linear algorithms include Linear Discriminant Analysis (LDA)[11, 12] and Principal Component Analysis (PCA)[13], and nonlinear algorithms include Kernel PCA, Isometric Feature Mapping, and Multi-dimensional Scaling (MDS) [14], etc. Feature selection algorithms select a portion of the original dimensions that are most important to the diagnosis and usually compute every feature's score independently, and then the top several scored features are selected. These methods include wrappers, filters, and hybrid (ensemble) methods[13]. Since the amount of monitoring data for mechanical systems, such as vibration data, is fairly large, the high computational cost poses a challenge for real-time fault diagnosis. Meanwhile, the relatively poor recoverability of these dimensionality reduction methods hinders their implementation. Therefore, a data reduction method with low computational cost and high recoverability is desired for real-time fault diagnosis with massive monitoring data.

Besides, online sample update or online network training is necessary for fault diagnosis under variable working conditions. Recently, to maximize the use of massive monitoring data, data-driven fault diagnosis techniques, especially AI algorithms[15, 16], are becoming popular due to their robustness and adaptability. For example, artificial neural networks, including deep learning methods, are widely used[16, 17]. However, the online training of these models is complicated with high computational costs. Algorithms with fast online training capability for massive monitoring data are more suitable for fault diagnosis under variable working conditions.

To simplify the process of multisource sensor data fusion and online training sample update, and also reduce data dimension simultaneously, in this study, a data fusion, reduction, and fault diagnosis method based on compressed sensing is proposed. Based on the sensor data compression framework and novel Batch Matching Pursuit (BMP) algorithm, the proposed method realizes multisource sensor data fusion and compression simultaneously, before fault diagnosis.

The main contributions of this paper include three aspects. First, multisource monitoring data are compressed and fused synchronously and efficiently, and the compression/fusion process works well with filed data processing and edge computing. Second, the amount of data is reduced by compression. Also, these compressed data can be employed directly for fault diagnosis or pattern recognition, which improves computation efficiency. Finally, the reference or training samples can be updated or extended rapidly, without model or network retraining.

The remainder of this paper is organized as follows: In Section 2, the process of data fusion, data compression, and fault diagnosis method is introduced, and the BMP algorithm is described in detail. In Section 3, the effectiveness of the proposed method is demonstrated in two cases. In Section 4, the conclusions of the study are presented.

2 Methodology

The architecture of this study is shown in Figure 1. The multisource sensor data are first compressed using a measurement matrix, and the data fusion process is conducted at the same time. Then, the compressed data are used for fault diagnosis, based on batch matching pursuit, reconstruction quality evaluation, and compressed reference matrix. The reference matrix is composed of multisource sensor data samples with different patterns and can be updated online, which is more suitable for fault diagnosis under variable working conditions. Since the reference matrix and the multisource sensor data are both compressed, the computational cost is significantly reduced, and the proposed BMP algorithm is more efficient than the Orthogonal Matching Pursuit (OMP) algorithm.

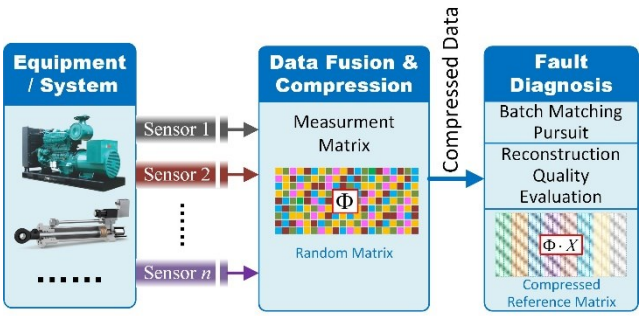

Figure 1 Architecture of the study

2.1 Compressed sensing and its application in monitoring data compression

Compressed sensing is a signal processing scheme for acquiring and reconstructing monitoring signals effectively, based on sparse representation[18]. The theory is based on the principle that, through optimization, a signal can be recovered from far fewer samples than required by the Shannon-Nyquist sampling theorem, by exploiting the sparsity of the signal [15][19]. The key parts of compressed sensing include measurement matrix, dictionary matrix and

reconstruction algorithm [16][20].

One of the conditions for compressed sensing is that the signal can be sparsely represented in a specific domain. For example, sparse representation for vibration monitoring signals acquired from rotating machinery can be achieved with a discrete Fourier transformation matrix[15]. Here, supposes the dictionary matrix is Ψ, then, the one-dimensional can be transformed to a sparse signal:

$$x = \Psi \cdot \theta \tag{1}$$

where x is a $N \times 1$ vector, Ψ is the dictionary matrix, and its size is $N \times N$, and θ is the sparse vector, and the size of θ is $N \times 1$.

Meanwhile, the monitoring signal is compressed using the measurement matrix Φ:

$$y = \Phi \cdot x \tag{2}$$

The size of Φ is $M \times N$ ($M \ll N$), thus, the original signal x is compressed to vector y, and its length is M.

Here, y is the compressed signal, and the purpose of compressed sensing is to reconstruct the original signal $\hat{x}$ from the compressed signal y:

$$y = \Phi \cdot \hat{x} \tag{3}$$

Based on Equation(3), the number of unkowns in $\hat{x}$ is N, and the number of linear equations in Equation(3) is M, since $M \ll N$, the reconstruction of the signal $\hat{x}$ from the signal y is an undetermined problem. However, with Equation(1) and Equation(2), the reconstruction is represented as

$$y = \Phi \cdot \hat{x} = \Phi \cdot \Psi \cdot \hat{\theta} \tag{4}$$

Here, $\hat{\theta}$ is a sparse vector and is estimated using Equation(4), based on the optimization algorithm. Later, the original signal can be reconstructed as follow:

$$\hat{y} = \Psi \cdot \hat{\theta} \tag{5}$$

To reconstruct the signal accurately, the measurement matrix Φ and the dictionary matrix Ψ should be uncorrelated, and the measurement matrix Φ is always a random matrix[21].

2.2 Fault diagnosis based on data fusion and compression

Based on compressed sensing theory and the presented BMP algorithm in this study, the main process of the study is illustrated in Figure 2. In this study, to achieve the goal of fault diagnosis, the dictionary matrix Ψ is constructed with labeled multisource sensor data, and the dictionary matrix Ψ is defined as the original reference matrix.

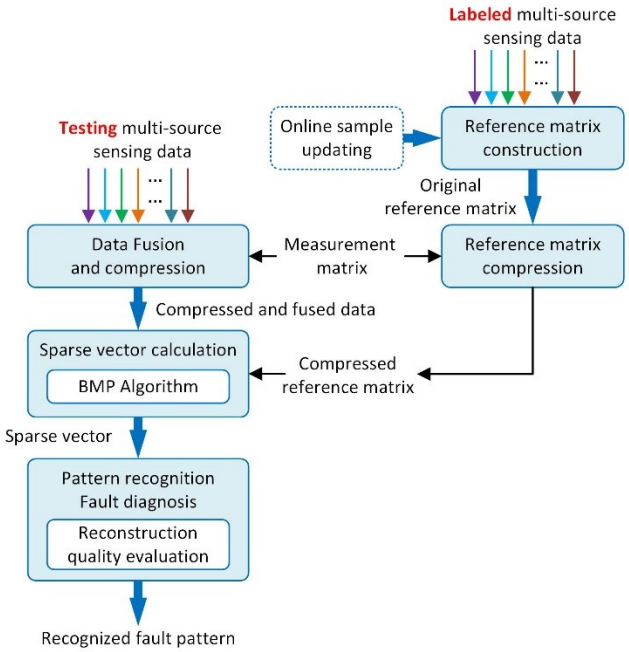

Figure 2 Fault diagnosis process

2.2.1 Reference matrix construction, data fusion, and compression

(1) Original reference matrix construction

As shown in Figure 2, the reference matrix is composed of labeled multisource sensor data segments with all patterns. Suppose the number of patterns (normal or fault) is p, and the number of data sources is s, then, the Original Reference Matrix (ORM) is:

$$X = \begin{pmatrix} X_{11} & X_{12} & \cdots & X_{1p} \\ X_{21} & X_{22} & \cdots & X_{2p} \\ \vdots & \vdots & \ddots & \vdots \\ X_{s1} & X_{s2} & \cdots & X_{sp} \end{pmatrix} \tag{6}$$

In Equation(6), $X_{ij}, i=1,2,\cdots,s, j=1,2,\cdots,p$ is a matrix and its size is $f_S \cdot t_S \times n_{DS}$, where f_S is the sampling frequency, t_S is sampling duration, and n_{DS} is the number of data samples in a single pattern, the size of X is $f_S \cdot t_S \cdot s \times n_{DS} \cdot p$, as shown in Figure 3.

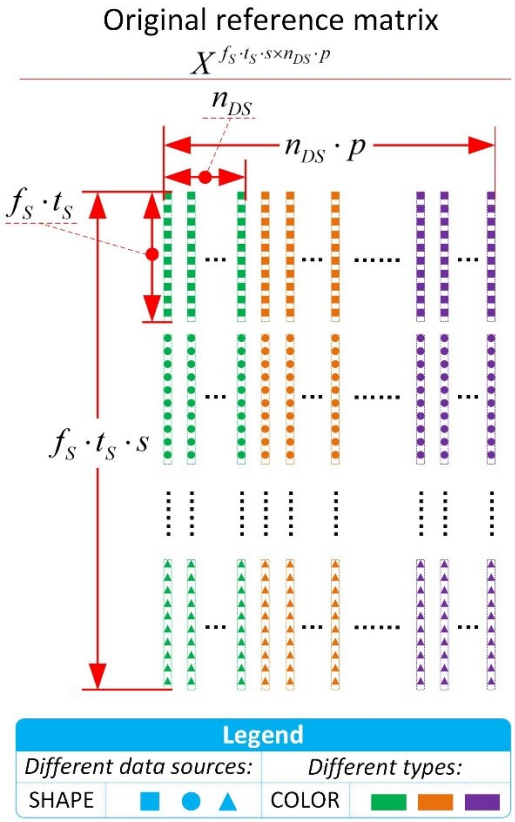

Figure 3 Construction of Original Reference Matrix

(2) Original reference matrix compression

Then, the ORM is compressed with a measurement matrix. Here, the compressed ORM is defined as the Compressed Reference Matrix (CRM). The data fusion is also conducted during the compression under the premise that ORM is uncorrelated to the measurement matrix. Generally, random matrix is the most commonly used measurement matrix.

The CRM is denoted as matrix Y:

$$Y_{M \times n_{DS} \cdot p} = \Phi_{M \times f_S \cdot t_S \cdot s} \cdot X_{f_S \cdot t_S \cdot s \times n_{DS} \cdot p} \tag{7}$$

Here, the compression ratio is $M/(f_S \cdot t_S \cdot s)$.

The measurement matrix Φ in Equation (7) is shown in Figure 4. Here, each row of the measurement matrix could be regarded as a fusion and a new resample for data samples collected from all original sources. Since arbitrary two rows of the measurement matrix are uncorrelated, all these resamples are non-redundant, and with a suitable compression ratio, these resamples covered nearly all information carried by the original multisources sensing data. Based on Equation (7), the CRM is demonstrated in Figure 5.

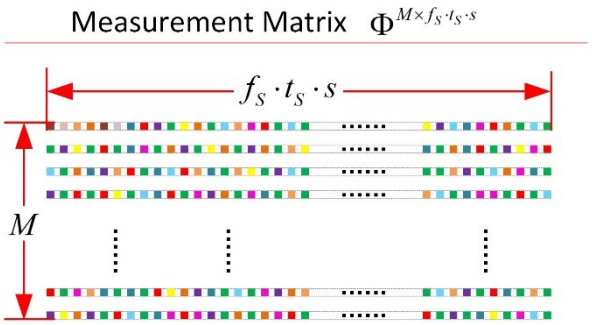

Figure 4 Measurement matrix

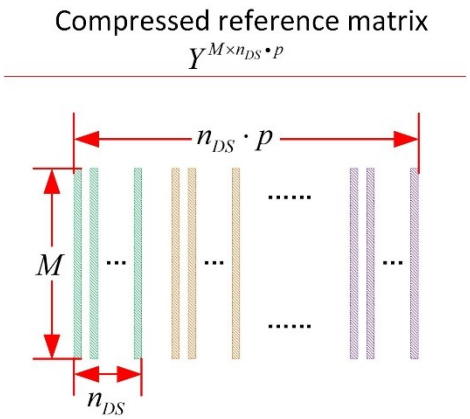

Figure 5 Compressed reference matrix

(3) Testing sample compression

To keep the consistency of vector structure, the testing sample v is also compressed with the same measurement matrix Φ:

$$z_{M \times 1} = \Phi_{M \times f_S \cdot t_S \cdot s} \cdot v_{f_S \cdot t_S \cdot s \times 1} \tag{8}$$

Here, column vector z is defined as compressed testing sample vector, and the structure of column vector z is the same as the structure of arbitrary column vector in CRM Y.

2.2.2 Adaptive classification vector calculation based on BMP algorithm

In this study, to improve calculation efficiency, as an improvement of orthogonal matching pursuit (OMP) algorithm[22], a new sparse vector calculation method, batch matching pursuit (BMP) algorithm is proposed. Details of the BMP algorithm are shown in Table 1.

Table 1 Batch matching pursuit algorithm

Input:

- Compressed reference matrix (CRM): $Y_{M\times n_{DS}\cdot p}$
- Compressed testing sample vector: $z_{M\times 1}$
- Number of patterns: p
- Number of support vectors in each batch: n_{SV}
- Number of iterations: n_{Iter}

Output:

- Sparse vector: $\hat{r}_{n_{DS}\cdot p\times 1}$

Intermediate Variables:

- Iteration counter: $times = 1,2,\cdots,n_{Iter}$
- Cosine similarity between vectors: *Product*
- Position index vector of nonzero elements in sparse vector: $\hat{r}_{Pos\ \ 1\times n_{SV}\cdot n_{Iter}}$
- Nonzero elements in sparse vector: $\hat{r}_{Element\ \ 1\times n_{SV}\cdot n_{Iter}}$
- Selected support vector set for compressed testing sample: $M_{SV\ \ M\times n_{SV}\cdot n_{Iter}}$
- Residual vector: *Res*

Procedures:

a. Initialization

Iteration counter: $times = 1$

Initial sparse vector: $\hat{r}_0 = \begin{pmatrix}0 & 0 & \cdots & 0\end{pmatrix}^T_{n_{DS}\cdot p\times 1}$

Position index vector of nonzero elements in sparse vector: $\hat{r}_{Pos,0} = [\ ]$

Initial residual vector: $Res_0 = z$

b. Calculation

Project the residual vector onto CRM to select those vectors in CRM that have the most significant contribution to the construction of the residual vector Res_0:

$$Product_{col} = \left(y_{col}^{\ T}\cdot Res_{times-1}\right)/\left(\left\|y_{col}\right\|\cdot\left\|Res_{times-1}\right\|\right) \tag{9}$$

y_{col} is the col^{th} column vector of CRM Y, and $col = 1,2,\cdots,n_{DS}\cdot p$.

select n_{SV} maximum values of $Product_{col}$, the position indices of these maximum n_{SV} values are:

$$\hat{r}_{Pos,times\ \ 1\times n_{SV}} = \left(col_1, col_2, \cdots, col_{n_{SV}}\right) \tag{10}$$

With the increasing of iteration counter *times*, The position index vector $\hat{r}_{Pos}$ is updated and extended with iteration demonstrated in Equation(10) and Equation(11):

$$\hat{r}_{Pos} = \hat{r}_{Pos}\bigcup\hat{r}_{Pos,times} \tag{11}$$

A batch of support vectors that contribute most in representing the compressed testing sample vector:

$$M_{SV,times} = Y_{\hat{r}_{Pos}} = Y\left(:,\hat{r}_{Pos}\right) \tag{12}$$

$M_{SV,times}$ is constructed by the column vectors that selected from Y, and the position indices of these column vectors are the elements of $\hat{r}_{Pos}$.

The column vectors in CRM Y, whose column indices are $\hat{r}_{Pos,times}$, are set to null vectors:

$$Y\left(:,\hat{r}_{Pos,times}\right) = 0 \tag{13}$$

The elements in sparse vector corresponding to the support vectors $M_{SV,times}$, $\hat{r}_{Element,times}$ are calculated by solving a least square problem, and the least square estimation method is employed here:

$$\hat{r}_{Element,times} = \left(M_{SV,times}^{\ T}\cdot M_{SV,times}\right)^{-1}\cdot M_{SV,times}^{\ T}\cdot z \tag{14}$$

After this process, the new residual vector Res_{times} is calculated:

$$Res_{times} = z - M_{SV,times}\cdot\hat{r}_{Element,times} \tag{15}$$

c. Iteration

The calculation procedures described with Equation(9) ~ Equation (15) are executed for n_{Iter} times repeatedly.

Then, the final position index vector $\hat{r}_{Pos}$ and final sparse vector elements vector $\hat{r}_{Element}$ are obtained, and sparse vector $\hat{r}$ is represented as:

$$\hat{r}_{n_{DS}\cdot p\times 1}:\ \hat{r}_{\hat{r}_{Pos}} = \hat{r}\left(\hat{r}_{Pos}\right) = \hat{r}_{Element} \tag{16}$$

Compared with the OMP algorithm, in the BMP algorithm, these support vectors used for testing sample construction are calculated in batch instead of one-by-one. Therefore, the calculation efficiency is improved, which is suitable for big data processing.

2.2.3 Pattern recognition based on reconstruction quality evaluation

Based on the BMP algorithm, vectors in the support vector set $M_{SV\ \ M\times n_{SV}\cdot n_{Iter}}$ represent the testing sample vector $z_{M\times 1}$ better than other vectors in the CRM. In other words, vectors in $M_{SV\ \ M\times n_{SV}\cdot n_{Iter}}$ are more similar to the compressed testing sample than others. Since the column vectors in CRM are grouped by the patterns of reference samples, and each element in the sparse vector corresponds to a column vector in the CRM, the values and positions of non-zero elements in the sparse vector indicate the pattern of the compressed testing sample. Therefore, in this study, the sparse vector is divided into p equal parts, and there are n_{DS} elements in each part, as shown in Figure 6, similarly, each part of the sparse vectors corresponds to a pattern of the CRM.

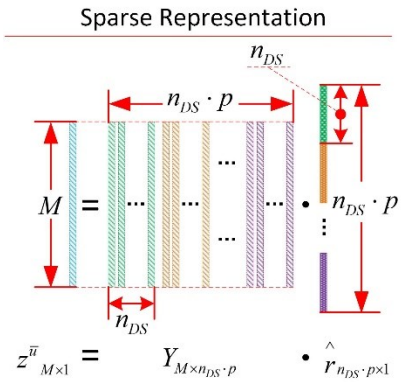

Figure 6 Sparse representation

Later, p derivate vectors are derived from the sparse vector, and for each derived vector, only one particular part of the sparse vector is retained, while other parts of the derivate vector are set to zero, as shown in Figure 7. After that, all the derived vectors are employed to reconstruct the compressed testing sample, by calculating the inner product of CRM and the derived vectors. Finally, compared with the compressed testing sample, the best reconstruction is selected, and the sequence number of non-zero parts in the corresponding derived vector, indicates the pattern of the compressed testing sample. Here, we define the above process as reconstruction quality evaluation.

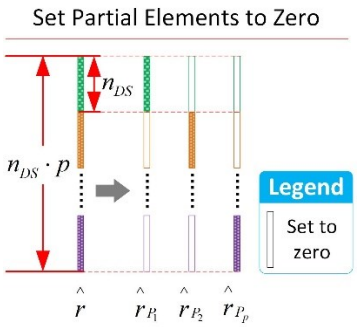

Figure 7 zero setting of sparse vector

The details of reconstruction quality evaluation are:

The elements of the sparse vector $\hat{r}$ are:

$$\hat{r} = \begin{pmatrix} r_1 & r_2 & \cdots & r_{n_{DS}} & \cdots \\ \cdots & r_{n_{DS}+1} & r_{n_{DS}+2} & \cdots & r_{2n_{DS}} & \cdots \\ & & \cdots & \cdots\cdots & \cdots & \\ \cdots & r_{(p-1)\cdot n_{DS}+1} & r_{(p-1)\cdot n_{DS}+2} & \cdots & r_{p\cdot n_{DS}} & \end{pmatrix}^T \tag{17}$$

Then, to eliminate the impact of match errors, except for the elements that correspond to the specific pattern, other elements in the sparse vector are set to zero, as shown in Equation (18) and Figure 7.

$$\begin{aligned}
\hat{r}_{P_1} &= \begin{pmatrix} r_1 & r_2 & \cdots & r_{n_{DS}} & \cdots \\ \cdots & 0 & 0 & \cdots & 0 & \cdots \\ & & \cdots & \cdots\cdots & \cdots & \\ \cdots & 0 & 0 & \cdots & 0 & \end{pmatrix}^T \\
\hat{r}_{P_2} &= \begin{pmatrix} r_1 & r_2 & \cdots & r_{n_{DS}} & \cdots \\ \cdots & 0 & 0 & \cdots & 0 & \cdots \\ & & \cdots & \cdots\cdots & \cdots & \\ \cdots & 0 & 0 & \cdots & 0 & \end{pmatrix}^T \\
&\vdots \qquad\qquad \vdots \\
\hat{r}_{P_p} &= \begin{pmatrix} & 0 & 0 & \cdots & 0 & \cdots \\ & \cdots & 0 & 0 & \cdots & 0 & \cdots \\ & & & \cdots & \cdots\cdots & \cdots & \\ \cdots & r_{(p-1)\cdot n_{DS}+1} & & r_{(p-1)\cdot n_{DS}+2} & \cdots & r_{p\cdot n_{DS}} & \end{pmatrix}^T
\end{aligned} \tag{18}$$

In Equation (18), $\hat{r}_{P_u}\ (u=1,2,\cdots,p)$ is the sparse vector that retains the elements corresponding to the positions of vectors in reference matrix CRM with a specific pattern.

The next step is to reconstruct the compressed test signal with $\hat{r}_{P_u}\ (u=1,2,\cdots,p)$, respectively:

$$\hat{z}_u = Y \cdot \hat{r}_{P_u} \quad (u=1,2,\cdots,p) \tag{19}$$

Finally, the reconstruction error is calculated as:

$$Err_u = \left\| z - \hat{z}_u \right\| \Big/ \|z\| \quad (u=1,2,\cdots,p) \tag{20}$$

Based on compressed sensing and sparse representation theory, with the CRM, the sparse vector which corresponds to the same pattern as the testing sample vector, could reconstruct the testing sample vector better than others. Therefore, the pattern of the testing sample is determined:

$$\text{Pattern} = u \ \ s.t. \min\left(Err_u\right) \ \ u=1,2,\cdots,p \tag{21}$$

2.3 Online sample updating and its application in fault diagnosis

With the increment of monitoring data quantity, more and more data samples with different patterns are recorded. In the conventionally used machine-learning-based fault diagnosis methods, model retraining is always required to maximize the use of these increased data samples, which consumes many computational resources. However, in this study, the reference matrix is composed of samples with different patterns (Figure 3), and the reference matrix could be extended and updated online.

As shown in Figure 8, the ORM can be updated by replacing any reference samples, or extended by adding $n_{EX} \cdot p$ new reference samples into it. Then, the updated or extended ORM is compressed and fused with the measurement matrix. Other diagnosis procedures are executed as Part 2.2 described without any changes. In terms of reference samples update and extension, the comparisons of compressed-sensing-based (CS-based) [23, 24]and machine-learning-based (ML-based) diagnosis methods[25, 26] are shown in Table 2. From this perspective, the method presented in this study is suitable for online fault diagnosis in field data processing and edge computing[27].

Table 2 Comparison of online training sampling update

	CS-based method	ML-based method
Feature extraction	Not required	Required
Model retraining	Not required	Required
Training parameter update	Not required	Required
Training time consumption	Low	High
Diagnosis time consumption	High	Low
Interpretability	High	Low

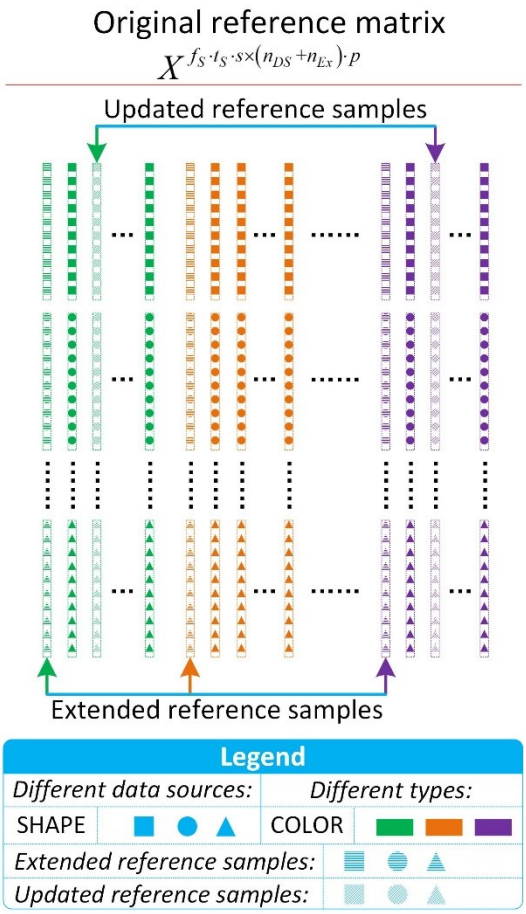

Figure 8 Reference samples update and extend

3 Case Study

3.1 Landfill gas power generator maintenance level recognition

3.1.1 Project background introduction

As shown in Figure 9, the LGPG consists of a twelve-cylinder V-type gas engine (left) and a three-phase brushless synchronous generator (right), and a shaft is supported by bearings. The type of the bearings is KOYO 6924C3, the speed of the shaft is 1000RPM.

Vibration data were collected using accelerometers, which were attached to the shaft house with magnetic bases and industrial glue. Three accelerometers were placed at the vertical direction, horizon direction and axis direction, marked as V direction, H direction and A direction, respectively. Vibration data were collected as a data file every 4 hours, and the sampling time of each file was 12 seconds, the sampling rate was 8000 data points per second.

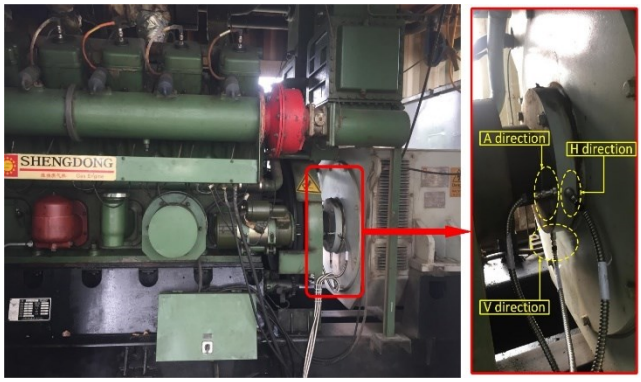

Figure 9 Landfill gas power generator

The project was started on July 1st, 2017, and lasted for two months. Nearly 4000 data files were collected. These data were used for maintenance pattern recognition. The collected data files were labeled as 'Normal', 'Maintenance', 'High-risk'. These labeled data samples were used for intelligent maintenance decision model training and condition-based maintenance.

3.1.2 Data sets description

In this case, 10 data files for each maintenance pattern were selected to validate the effectiveness of the algorithm, as shown in Table 3. As described above, three accelerometers were placed, the sampling time of each file was 12 seconds, and the sampling rate was $8KS/s$. Thus, each data file contains 96000×3 data points. Since the rotational speed of the shaft was 1000RPM, and the sample rate was $8KS/s$, then, 480×3 data points were collected during a shaft rotating cycle. In this case, a data sample contains two shaft rotating cycle, and the size of the data sample was 960×3, therefore, for each maintenance pattern, the data set contained1000 data samples.

Table 3 Data sets description

Maintenance Pattern	Number of data files	Number of data samples	Number of reference data samples	Number of test data samples
Normal	10	1000	750	250
Maintenance	10	1000	750	250
High-risk	10	1000	750	250
Total	30	3000	2250	750

Later, for each maintenance pattern, 750 data samples were employed to construct the reference matrix (Table 4), and the other 250 data samples were employed as test data samples (Table 5).

Table 4 Details of reference samples

Reference sample number	Column 1^{st}-750^{th}	Column 751^{th}-1500^{th}	Column 1501^{th}-2250^{th}
Pattern	Normal	Maintenance	High-risk
Accelerometer direction	Line 1^{st}-Line 960^{th}: Axis direction Line 961^{th}-Line 1920^{th}: Horizon direction Line 1921^{th}-Line 2880^{th}: Vertical direction		

Table 5 Details of testing samples

Testing sample number	Column 1^{st}-250^{th}	Column 251^{th}-500^{th}	Column 501^{th}-750^{th}
Pattern	Normal	Maintenance	High-risk
Accelerometer direction	Line 1^{st}-Line 960^{th}: Axis direction Line 961^{th}-Line 1920^{th}: Horizon direction Line 1921^{th}-Line 2880^{th}: Vertical direction		

3.1.3 Multisource sensor data processing

(1) Reference matrix construction and compression

First, for each data sample, vibration data collected from A/H/V directions were arranged longitudinally as a column vector, and these column vectors were grouped by maintenance patterns, as shown in Figure 3. In this case, the ORM was constructed by samples shown in Table 4 and is shown as a gray image in Figure 10.

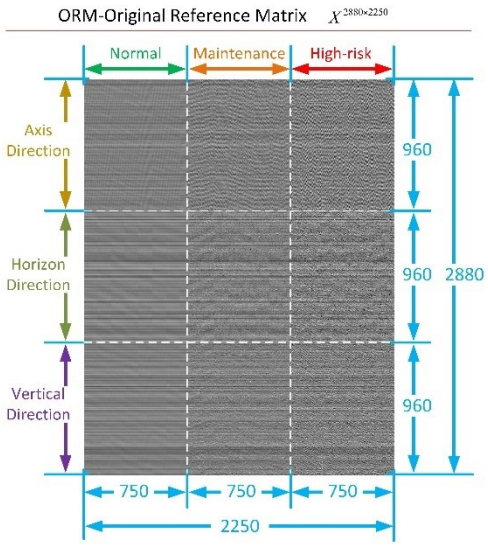

Figure 10 LGPG – ORM

Then, the ORM was compressed with a random matrix $\Phi^{1152\times2880}$ (shown in Figure 11), the compression ratio was $1152/2880=0.4$, and these data from different accelerometers were also fused during the process of compression, the CRM $Y^{1152\times2250}=\Phi^{1152\times2880}\cdot X^{2880\times2250}$ is shown in Figure 12.

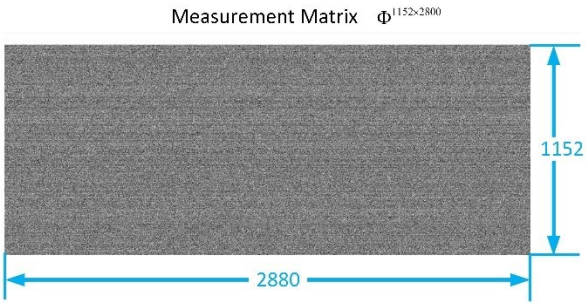

Figure 11 LGPG – Measurement matrix

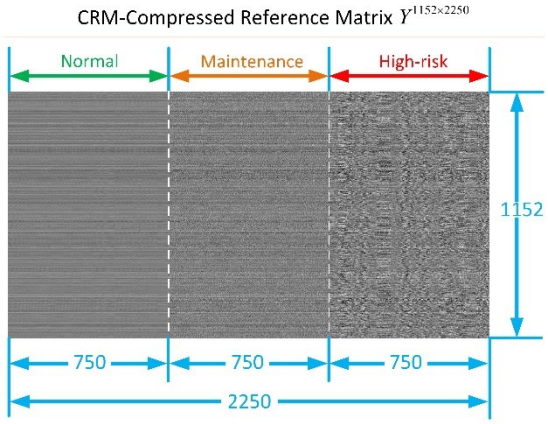

Figure 12 LGPG – CRM

(2) Sparse vector calculation

In this case, 750 testing samples were selected to validate the algorithm, as shown in Table 5, before the calculation of sparse vector, these testing samples were also compressed with measurement matrix Φ. Then, the sparse vectors were calculated with the BMP algorithm, and the number of support vectors in each batch was 3, the number of iterations was 3, therefore, each sparse vector contained 9 non-zero elements. For each testing sample, the size of sparse vector was 2250×1, and the elements in the sparse vector corresponded to the column vectors in the CRM. The sparse vectors of all 750 testing samples composed a matrix $M_{sparse}^{2250\times750}$, the matrix was shown in Figure 13, in this image, white points are non-zero elements.

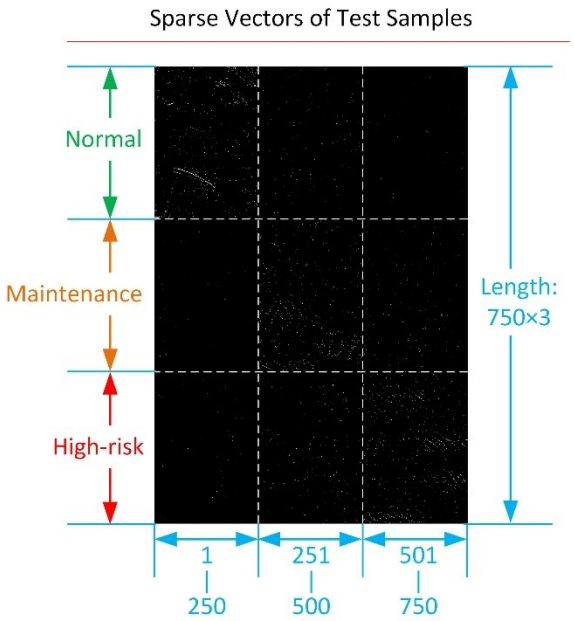

Figure 13 LGPG - Sparse vectors

From Figure 13, we found that the positions of most non-zero elements in the sparse vector were determined by the pattern of the testing sample and the arrangement of the CRM. To discuss the relationship between the non-zero elements in sparse vector and the arrangement of CRM, sparse vectors that corresponded to testing samples with different patterns are shown in Figure 14.

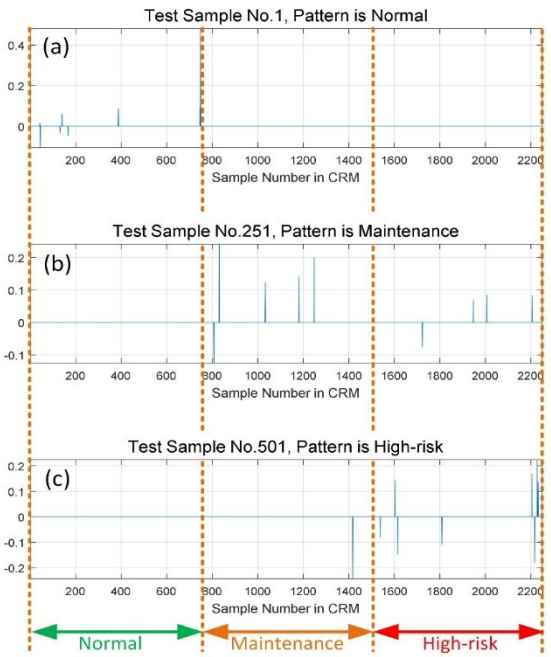

Figure 14 LGPG - Sparse vectors

Figure 14 (a) is the sparse vector calculated from the first testing sample, and the pattern of this testing sample was normal, in this sparse vector, most of none-zero elements (43th, 45th, 132th, 141th, 167th, 388th, 746th, 749th, 750th) lay in 1st-750th elements, which corresponded to normal reference samples in the CRM, and the absolute values of these elements were greater than others. This means that the 1st compressed testing sample were most similar to the 43th, 45th, 132th, 141th, 167th, 388th, 746th, 749th, 750th compressed reference samples. This conclusion was also tenable for Figure 14 (b) and Figure 14 (c).

(3) Reconstruction evaluation and pattern recognition

In this part, the testing sample No.1, No.251 and No.501 were reconstructed with $\hat{r}_{\text{Normal}}$, $\hat{r}_{\text{Maintenance}}$ and $\hat{r}_{\text{High-risk}}$, respectively, and shown in Figure 15, Figure 16 and Figure 17.

Figure 15 is the reconstruction of No.1 compressed testing sample, since all the 9 non-zero elements in sparse vector lay in 1st – 750th elements, the estimated signal reconstructed with $\hat{r}_{\text{Maintenance}}$ and $\hat{r}_{\text{High-risk}}$ were zero signals, obviously, the reconstruction error Err_{Normal} was minimum, thus, the pattern of this testing sample was Normal.

Figure 16 is the reconstruction of No.251 compressed testing sample. The blue dashed curve in Figure 16 (b) was the estimated signal with $\hat{r}_{\text{Maintenance}}$, although it was different from the red curve (compressed test signal), it was the most similar curve with the red curve among Figure 16 (a), Figure 16 (b) and Figure 16 (c), in other words, the reconstruction error $Err_{\text{Maintenance}}$ was minimum, therefore, the pattern of testing sample No.251 was Maintenance.

Figure 17 shows the reconstruction of testing sample No.501. Similarly, the reconstruction error of Figure 17 (c) was the smallest, thus, the maintenance pattern of this testing sample was High-risk.

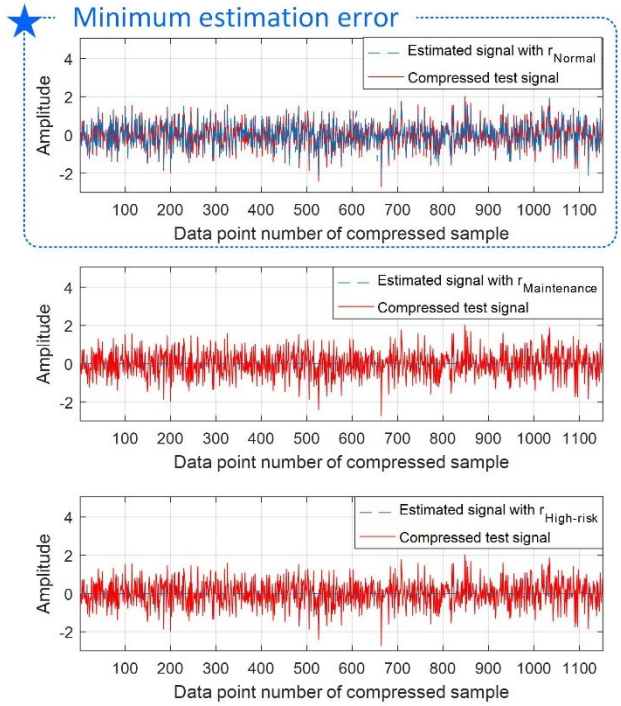

Figure 15 LGPG - Compressed testing sample reconstruction (Normal)

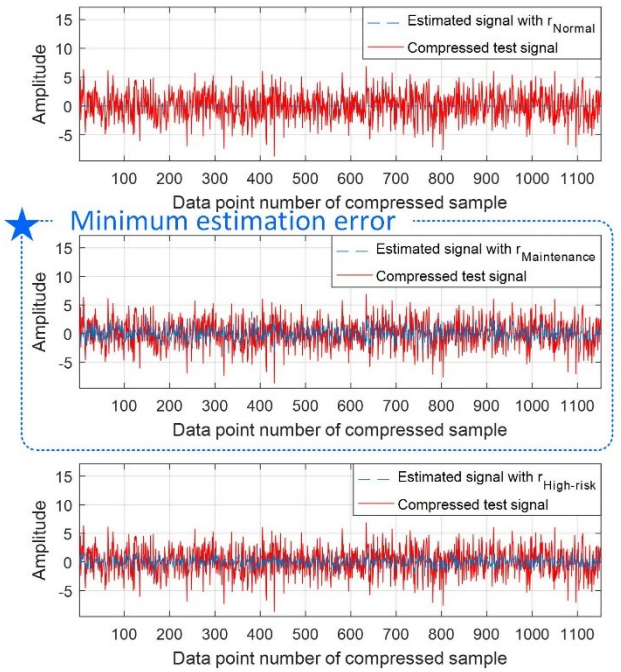

Figure 16 LGPG - Compressed testing sample reconstruction (Maintenance)

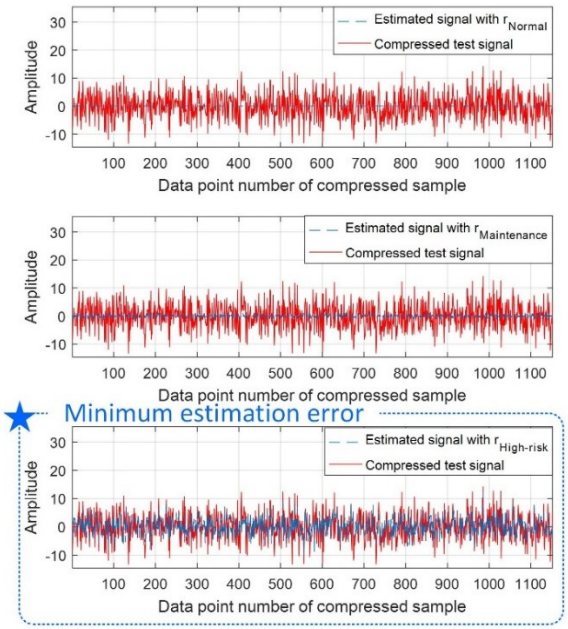

Figure 17 LGPG - Compressed testing sample reconstruction (High-risk)

3.1.4 Result analysis

To validate the effectiveness of the proposed algorithm, more testing samples listed in Table 5 were processed. The maintenance recognition results of the testing samples were obtained based on the proposed method. Since these testing samples were fetched from the LGPG historical monitoring data, their maintenance patterns were predetermined, as shown in the 2nd line of Table 5, that is, the maintenance pattern of the 1st-250th testing sample is NORMAL, the maintenance pattern of the 251th-500th testing sample is MAINTENANCE, and the maintenance pattern of the 501th-750th testing sample is HIGH-RISK. The recognition results and theoretical results (predetermined maintenance pattern) were expressed with Figure 18, and 721 testing samples were recognized correctly, thus, the corresponding maintenance pattern recognition accuracy was 96.13%.

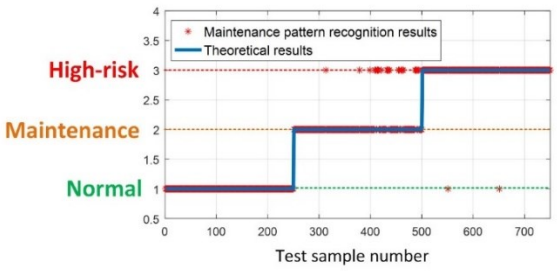

Figure 18 LGPG - Maintenance pattern recognition results

3.2 Multiple redundancy aileron actuator fault diagnosis

3.2.1 Simulation model introduction

MRAA is a key component of a flight control system, which is widely used in nearly all kinds of aircraft. An MRAA could have numerous faults, including sensor, force motor, and actuator leakage faults, whose diagnosis and timely handing could increase flying safety. In this study, a simulation model of MRAA was established to generate simulation data.

A four-redundancy aileron actuator consisting of four Proportion-Integration-Differentiation (PID) controllers, four amplifiers, four sensors, a servo valve, and a cylinder, was simulated with MATLAB Simulink and AMESim. The control part of the MRAA was established in Simulink, and the mechanical part was established in AMESim, as shown in Figure 19.

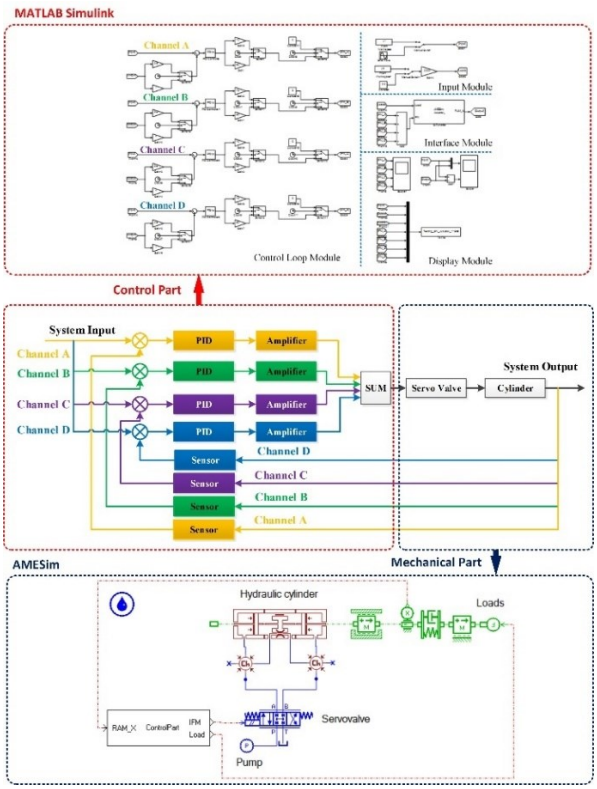

Figure 19 MRAA simulation model

Different faults were introduced by changing the key parameters of the simulation model, and the details of fault injection are shown in Table 6.

Table 6 Details of fault injection

Test No.	(Fault) Pattern	Fault channel	Changed parameter for fault injection (unit)	Parameter (Normal)	Parameter (Fault)
1	Normal	-	-	-	-
2	Force motor fault	A	FMC gain (none)	1	0
3	Force motor fault	B	FMC gain (none)	1	0
4	Sensor fault	A	Signal output (1/m)	1	0.8
5	Sensor fault	B	Signal output (1/m)	1	0.8
6	Internal leakage	-	Piston leakage diameter (mm)	1e-5	1.0

Comments:
Force motor fault means a force motor coil disconnection fault
Sensor fault means an inter-turn short circuit fault of sensor induction coil
Internal leakage means a hydraulic cylinder internal leakage fault

Based on industrial application, in this case, seven data sources, including system input, system output, force motor current (Channel A, B, C, D), and aerodynamic loads, were collected from the simulation model, and the sampling rate was 10S/s.

3.2.2 *Data sets description*

In this case study, for each pattern, the simulation was lasted for 240 seconds, and 2400×7 data points for each pattern were collected. Then, every 80×7 data points were defined as a data sample, thus, for each pattern, the data points were divided into 30 data samples.

Table 7 Data sets description

(Fault) Pattern (Abbr.)	Simulation time (s)	Number of data samples	Number of reference data samples	Number of test data samples
Normal (Normal)	240	30	20	10
Channel A Force motor fault (FM_A)	240	30	20	10
Channel B Force motor fault (FM_B)	240	30	20	10
Channel A Sensor fault (S_A)	240	30	20	10
Channel B Sensor fault (S_B)	240	30	20	10
Internal Leakage (IL)	240	30	20	10
Total	1440	180	120	60

Later, for each pattern, 20 data samples were employed to construct the reference matrix, while the other 10 data segments were employed as testing samples, as shown in Table 8.

Table 8 Details of reference and testing samples

Pattern	Normal	FM_A	FM_B	S_A	S_B	IL
Reference sample number (Column)	1st-20th	21th-40th	41th-60th	61th-80th	81th-100th	101th-120th
Testing sample number (Column)	1st-10th	11th-20th	21th-30th	31th-40th	41th-50th	51th-60th
Signal source	Line 1st-80th: System input Line 81th-160th: System output Line 161th-240th: Aerodynamic loads Line 241th-320th: Force motor current of channel A Line 321th-400th: Force motor current of channel B Line 401th-480th: Force motor current of channel C Line 481th-560th: Force motor current of channel D					

3.2.3 *Multisource sensor data processing*

(1) Reference matrix construction and compression

In this case, data collected from seven different signal sources were arranged end-to-end as a column vector of ORM $X^{560\times120}$, the length of the column vector was $80\times7=560$, as shown in Table 8. Then, these column vectors, shown in Table 8, were grouped by patterns and constitute the ORM $X^{560\times120}$. To save space, the ORM was transposed and shown as a gray image in Figure 20.

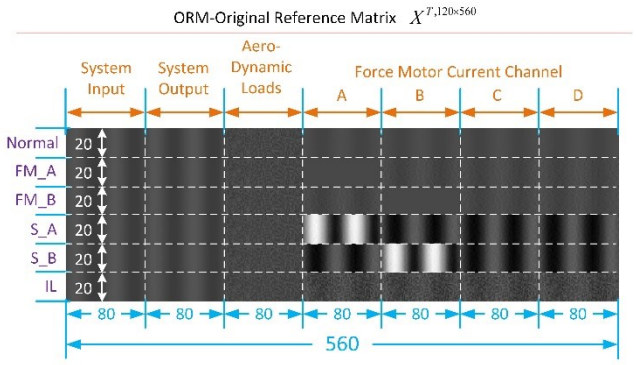

Figure 20 Transpose of MRAA – ORM

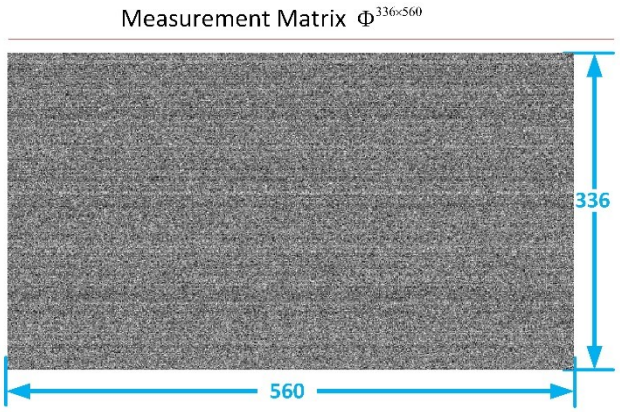

Figure 21 MRAA – Measurement matrix

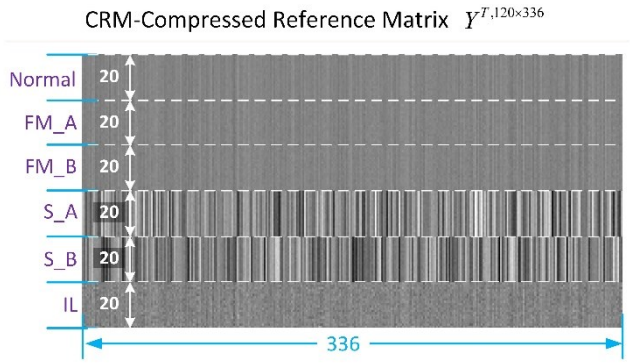

Figure 22 Transpose of MRAA - CRM

Later, the ORM was compressed with a random measurement matrix $\Phi^{336\times560}$ (Figure 21), and these data from different sources were also fused at the same time, the compression ratio was $336/560=0.6$, the CRM is shown in Figure 22.

$$Y^{336\times120}=\Phi^{336\times560}\cdot X^{560\times120} \tag{22}$$

(2) Sparse vector calculation

As shown in Table 8, 60 test data samples, consisting of system input, system output, aerodynamic loads and force motor currents, were employed to validate the algorithm. These testing samples were also compressed with the measurement matrix $\Phi^{336\times560}$ before the sparse vector calculation. Later, the sparse vectors of these testing samples were calculated with the proposed BMP algorithm, and the number of support vectors in each batch was 4, the number of iterations was 3, thus, each sparse vector contained 12 non-zero elements. Since the number of reference sample vectors in the CRM was 120, the size of sparse vector in this case was 120×1, each element in sparse vector corresponded to one reference sample column vector in CRM. The sparse vectors of all 60 testing samples composed a matrix $M_{sparse}^{120\times60}$, and the matrix was transposed and shown in Figure 23, where the white points are non-zero elements.

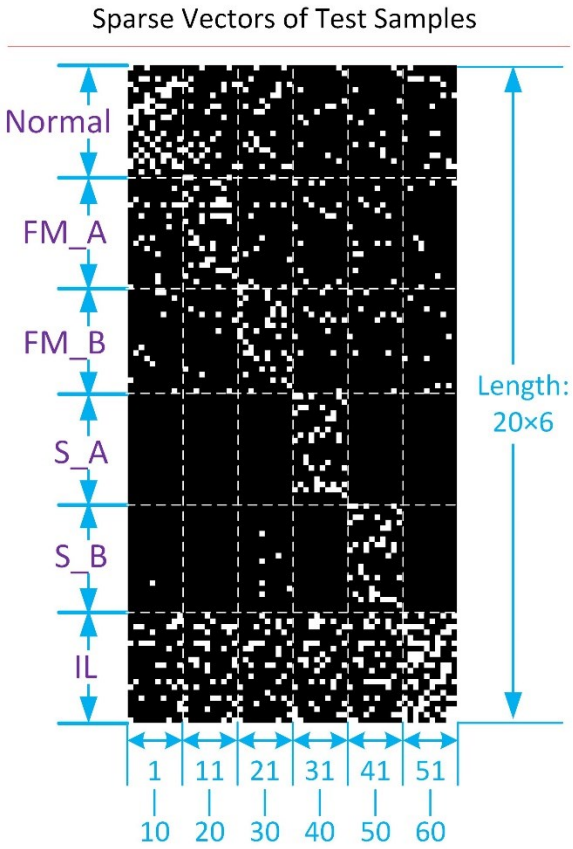

Figure 23 MRAA – Sparse vectors

As shown in Figure 23, the locations of non-zero elements in the sparse vectors indicated the (fault) patterns of the testing sample. For example, in the sparse vectors of the 1st-10th testing samples, most of the non-zero elements located in the 1st-20th lines. Then, to show the details of sparse vector, several sparse vectors with different patterns are shown in Figure 24.

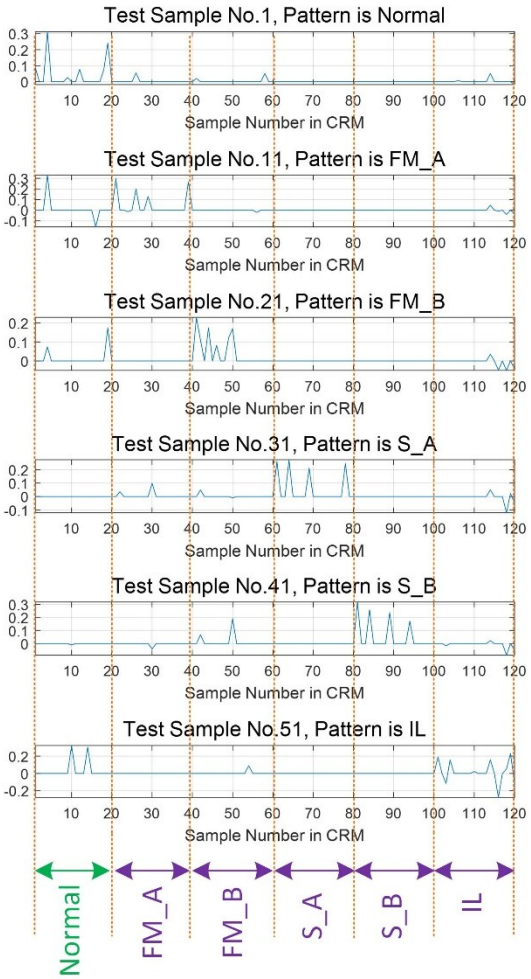

Figure 24 MRAA – Adaptive classification vectors

The first curve in Figure 24 is the sparse vector calculated from the first testing sample, and the pattern was normal, in this figure, half of the non-zero elements (1st, 4th, 9th, 12th, 18th, 19th) lay in 1st-20th, and corresponded to normal reference vectors in CRM, meanwhile, the values of these elements were greater than others. In other words, based on the BMP algorithm, among all these reference vectors in CRM, the 1st testing sample was most similar with the 1st, 4th, 9th, 12th, 18th, 19th reference vectors. Similarly, the principle was also approved in other curves.

(3) Reconstruction evaluation and pattern recognition

In this part, to save space, only testing sample No.1 (Normal) and testing sample No.51 (IL, actuator leakage fault) were reconstructed with $\hat{r}_{Normal}$, $\hat{r}_{FM\_A}$, $\hat{r}_{FM\_B}$, $\hat{r}_{S\_A}$, $\hat{r}_{S\_B}$, and $\hat{r}_{IL}$, respectively, then, these reconstructed signals ($\hat{z}_{Normal}$, $\hat{z}_{FM\_A}$, $\hat{z}_{FM\_B}$, $\hat{z}_{S\_A}$, $\hat{z}_{S\_B}$ and $\hat{z}_{IL}$) were compared with the compressed signals z.

Figure 25 is the reconstruction of No.1 compressed testing sample, and the pattern of this sample was Normal. As shown in the first curve of Figure 24, most non-zero elements in sparse vector lay in the area corresponding to the Normal pattern, therefore, the estimated signal with $\hat{r}_{Normal}$ (Figure 25 (a)) was most similar to the compressed test signal.

Similarly, in Figure 26, the testing sample was reconstructed with $\hat{r}_{Normal}$, $\hat{r}_{FM\_A}$, $\hat{r}_{FM\_B}$, $\hat{r}_{S\_A}$, $\hat{r}_{S\_B}$, and $\hat{r}_{IL}$, respectively, and the estimated signal based on $\hat{r}_{IL}$ was most similar to the compressed test signal, as shown in Figure 26 (f), therefore, the pattern of this testing sample was leakage fault.

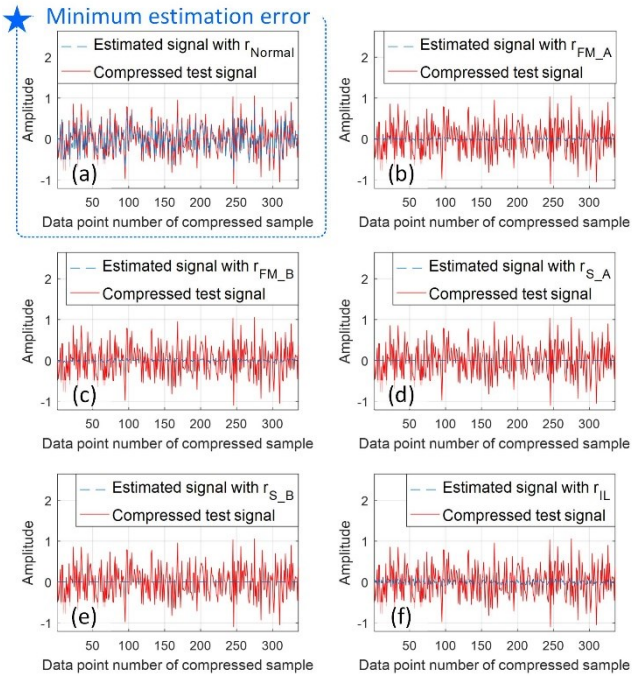

Figure 25 MRAA – Compressed testing sample reconstruction (Normal)

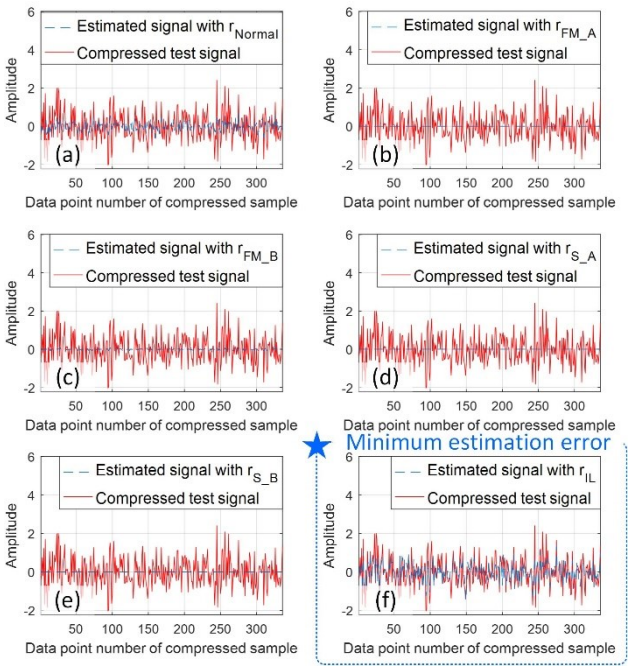

Figure 26 MRAA – Compressed testing sample reconstruction (Leakage fault)

3.2.4 Result analysis

To validate the effectiveness of the proposed method with the MRAA simulation data, the test results of all 60 testing samples were expressed in Figure 27. Here, the theoretical results were the predetermined labels of the testing samples, as shown in the 2nd line of Table 8. Among these 60 testing samples, two testing samples (FM_A and IL) were mistakenly recognized as Normal, and the pattern recognition accuracy was 96.67%.

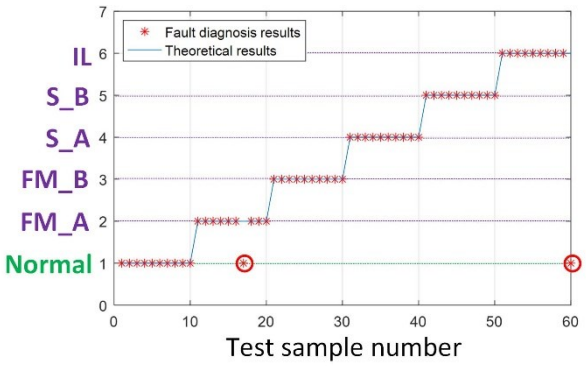

Figure 27 MRAA – Fault diagnosis results

4 Conclusions

In this study, based on compressed sensing theory, a fault diagnosis method with multisource sensor data is presented. First, an ORM is constructed with labeled samples, each labeled sample is a column vector which is composed of data collected from different sources, and these labeled samples are arranged horizontal and grouped by patterns. Then, the ORM is compressed with a measurement matrix, and the multisource sensor data are fused synchronously. Later, before the process of fault diagnosis, the testing sample is also compressed and fused with the measurement matrix, and the compressed testing sample is obtained. After that, the compressed testing sample is sparsely represented with the compressed reference matrix (CRM), based on the BMP algorithm proposed in this study, and a sparse vector is calculated. Since the value and the position of the nonzero elements in the sparse vector indicate the pattern of the compressed testing sample, in this study, for a particular pattern, a derived vector is obtained by retaining elements that corresponded to the particular pattern exclusively and setting other elements to zero. Finally, for each pattern, an estimated testing sample is reconstructed with the CRM and the corresponding derivate vector, by comparing these estimated testing samples and the compressed testing sample, the pattern of the estimation with minimum error is the pattern to be determined.

To validate the effectiveness of the proposed fault diagnosis method, two tests were carried out. In the first case, multisource acceleration data were acquired from different directions of an LGPG, with these multisource sensor data, the maintenance pattern was determined based on the proposed method in this study, and the recognition accuracy was 96.13%. The other case is the fault diagnosis of an MRAA based on multiple monitoring data, including system input, system output, force motor current, etc.. Based on the proposed fault diagnosis method, the diagnosis accuracy was 96.67%.

The advances of the proposed method include three aspects. First, the fusion and compression of multisource sensor data fusion are carried out simultaneously, and this process is based on an inner product operation simply, which is an ideal data fusion method for field data processing or edge computing, the application scenarios include but are not limited to the industrial field, automobile industry, or aerospace. Second, these compressed data can be employed for fault diagnosis or pattern recognition based on sparse representation scheme directly, without feature extraction and model training, therefore, the diagnosis scheme can be deployed and implemented in SoC, such as ARM platform, thus, the proposed method can be widely applied to portable devices, such as portable maintenance assistant, or

onboard fault diagnosis system. Finally, the reference samples could be updated and extended rapidly, and the updated or extended ORM can be used for fault diagnosis directly, which make it more suitable for isolated or off-line fault diagnosis system, such as health management system in ship, submarine, or spacecraft.

However, the criteria of reference samples extension or update should be determined based on sample validity evaluation, and the evaluation method will be further developed. Besides, how to improve the efficiency of sparse representation dealing with large-scale ORM, should be solved in future works. Finally, in some cases, the numbers of reference labeled samples of different patterns are not same, thus, the proposed method will be improved, and the reference samples in the ORM could be adjusted adaptively.

5 Declaration

Acknowledgements

Not applicable

Funding

Supported by National Natural Science Foundation of China (Grant Nos.51875054, U1864212), Chongqing Municipal Natural Science Foundation for Distinguished Young Scholars of China (Grant No.cstc2019jcyjjqX0016), Chongqing Science and Technology Bureau of China.

Availability of data and materials

The datasets used and analyzed during the current study are available from the corresponding author on reasonable request.

Authors' contributions

XY was in charge of the whole trial; XY and KZ wrote the manuscript; HY provided the simulation model. All authors read and approved the final manuscript.

Competing interests

The authors declare no competing financial interests.

Consent for publication

Not applicable

Ethics approval and consent to participate

Not applicable

References

[1] M. Huang, Z. Liu, and Y. Tao, "Mechanical Fault Diagnosis and Prediction in IoT Based on Multi-source Sensing Data Fusion," *Simulation Modelling Practice and Theory,* p. 101981, 2019/09/03/ 2019, doi: https://doi.org/10.1016/j.simpat.2019.101981.

[2] K. Moharm, "State of the art in big data applications in microgrid: A review," *Advanced Engineering Informatics,* vol. 42, p. 100945, 2019/10/01/ 2019, doi: https://doi.org/10.1016/j.aei.2019.100945.

[3] Q. Liu, D. Kong, S. J. Qin, and Q. Xu, "Map-Reduce Decentralized PCA for Big Data Monitoring and Diagnosis of Faults in High-Speed Train Bearings**Support to this research was provided by the Natural Science Foundation of China (61490704, 61673097, 61573022), the Fundamental Research Funds for the Central Universities (N160804002, N160801001), the Fundamental Disciplinary Research Program of the Shenzhen Committee on Science and Innovation (20160207), and the Texas-Wisconsin-California Control Consortium (TWCCC)," *IFAC-PapersOnLine,* vol. 51, no. 18, pp. 144-149, 2018/01/01/ 2018, doi: https://doi.org/10.1016/j.ifacol.2018.09.290.

[4] G. Qi, Z. Zhu, K. Erqinhu, Y. Chen, Y. Chai, and J. Sun, "Fault-diagnosis for reciprocating compressors using big data and machine learning," *Simulation Modelling Practice and Theory,* vol. 80, pp. 104-127, 2018/01/01/ 2018, doi: https://doi.org/10.1016/j.simpat.2017.10.005.

[5] Z. Pan, Z. Meng, Y. Zhang, G. Zhang, and X. Pang, "High-precision bearing signal recovery based on signal fusion and variable stepsize forward-backward pursuit," *MECHANICAL SYSTEMS AND SIGNAL PROCESSING,* Article vol. 157, 2021 AUG 2021, doi: 10.1016/j.ymssp.2021.107647.

[6] Z. Xuewei and L. Hanshan, "Research on transformer fault diagnosis method and calculation model by using fuzzy data fusion in multi-sensor detection system," *Optik,* vol. 176, pp. 716-723, 2019/01/01/ 2019, doi: https://doi.org/10.1016/j.ijleo.2018.09.017.

[7] W. Fu, J. Tan, X. Zhang, T. Chen, and K. Wang, "Blind parameter identification of MAR model and mutation hybrid GWO-SCA optimized SVM for fault diagnosis of rotating machinery," *Complexity,* vol. 2019, 2019.

[8] H. Huang, B. Tang, J. Luo, H. Pu, and K. Zhang, "Residual Gated Dynamic Sparse Network for Gearbox Fault Diagnosis Using Multisensor Data," *IEEE TRANSACTIONS ON INDUSTRIAL INFORMATICS,* Article vol. 18, no. 4, pp. 2264-2273, 2022 APR 2022, doi: 10.1109/TII.2021.3099060.

[9] M. Sun, H. Wang, P. Liu, S. Huang, P. Wang, and J. Meng, "Stack Autoencoder Transfer Learning Algorithm for Bearing Fault Diagnosis Based on Class Separation and Domain Fusion," *IEEE TRANSACTIONS ON INDUSTRIAL ELECTRONICS,* Article vol. 69, no. 3, pp. 3047-3058, 2022 MAR 2022, doi: 10.1109/TIE.2021.3066933.

[10] Y. Gong, X. Su, H. Qian, and N. Yang, "Research on fault diagnosis methods for the reactor coolant system of nuclear power plant based on D-S evidence theory," *Annals of Nuclear Energy,* vol. 112, pp. 395-399, 2018/02/01/ 2018, doi: https://doi.org/10.1016/j.anucene.2017.10.026.

[11] Y. Zhou, S. Yan, Y. Ren, and S. Liu, "Rolling bearing fault diagnosis using transient-extracting transform and linear discriminant analysis," *MEASUREMENT,* Article vol. 178, 2021 JUN 2021, doi: 10.1016/j.measurement.2021.109298.

[12] Q. Song, S. Zhao, and M. Wang, "On the Accuracy of Fault Diagnosis for Rolling Element Bearings Using Improved DFA and Multi-Sensor Data Fusion Method," *SENSORS,* Article vol. 20, no. 22, 2020 NOV 2020, doi: 10.3390/s20226465.

[13] X. Xu, T. Liang, J. Zhu, D. Zheng, and T. Sun, "Review of classical

dimensionality reduction and sample selection methods for large-scale data processing," *Neurocomputing,* vol. 328, pp. 5-15, 2019/02/07/ 2019, doi: https://doi.org/10.1016/j.neucom.2018.02.100.

[14] H. Zhang, H. Chen, Y. Guo, J. Wang, G. Li, and L. Shen, "Sensor fault detection and diagnosis for a water source heat pump air-conditioning system based on PCA and preprocessed by combined clustering," *Applied Thermal Engineering,* vol. 160, p. 114098, 2019/09/01/ 2019, doi: https://doi.org/10.1016/j.applthermaleng.2019.114098.

[15] Z. Wu, H. Jiang, K. Zhao, and X. Li, "An adaptive deep transfer learning method for bearing fault diagnosis," *Measurement,* vol. 151, p. 107227, 2020/02/01/ 2020, doi: https://doi.org/10.1016/j.measurement.2019.107227.

[16] R. Liu, B. Yang, E. Zio, and X. Chen, "Artificial intelligence for fault diagnosis of rotating machinery: A review," *Mechanical Systems and Signal Processing,* vol. 108, pp. 33-47, 2018/08/01/ 2018, doi: https://doi.org/10.1016/j.ymssp.2018.02.016.

[17] D.-T. Hoang and H.-J. Kang, "A survey on Deep Learning based bearing fault diagnosis," *Neurocomputing,* vol. 335, pp. 327-335, 2019/03/28/ 2019, doi: https://doi.org/10.1016/j.neucom.2018.06.078.

[18] M. Elad, "Optimized projections for compressed sensing," *IEEE TRANSACTIONS ON SIGNAL PROCESSING,* Article vol. 55, no. 12, pp. 5695-5702, 2007 DEC 2007, doi: 10.1109/TSP.2007.900760.

[19] E. J. Candes, Y. C. Eldar, D. Needell, and P. Randall, "Compressed sensing with coherent and redundant dictionaries," *APPLIED AND COMPUTATIONAL HARMONIC ANALYSIS,* Article vol. 31, no. 1, pp. 59-73, 2011 JUL 2011, doi: 10.1016/j.acha.2010.10.002.

[20] Z. Zhang, Y. Xu, J. Yang, X. Li, and D. Zhang, "A Survey of Sparse Representation: Algorithms and Applications," *IEEE ACCESS,* Article vol. 3, pp. 490-530, 2015 2015, doi: 10.1109/ACCESS.2015.2430359.

[21] J. A. Tropp and A. C. Gilbert, "Signal recovery from random measurements via orthogonal matching pursuit," *IEEE TRANSACTIONS ON INFORMATION THEORY,* Article vol. 53, no. 12, pp. 4655-4666, 2007 DEC 2007, doi: 10.1109/TIT.2007.909108.

[22] S. K. Chaitanya and K. Srinivasan, "Equivalent source method based near field acoustic holography using multipath orthogonal matching pursuit," *APPLIED ACOUSTICS,* Article vol. 187, 2022 FEB 2022, doi: 10.1016/j.apacoust.2021.108501.

[23] X. Pei, X. Zheng, and J. Wu, "Intelligent bearing fault diagnosis based on Teager energy operator demodulation and multiscale compressed sensing deep autoencoder," *MEASUREMENT,* Article vol. 179, 2021 JUL 2021, doi: 10.1016/j.measurement.2021.109452.

[24] D. Han, J. Yu, M. Gong, Y. Song, and L. Tian, "A Remaining Useful Life Prediction Approach Based on Low-Frequency Current Data for Bearings in Spacecraft," *IEEE SENSORS JOURNAL,* Article vol. 21, no. 17, pp. 18978-18989, 2021 SEPT 1 2021, doi: 10.1109/JSEN.2021.3086677.

[25] Y. Wen, M. F. Rahman, H. Xu, and T.-L. B. Tseng, "Recent advances and trends of predictive maintenance from data-driven machine prognostics perspective," *MEASUREMENT,* Article vol. 187, 2022 JAN 2022, doi: 10.1016/j.measurement.2021.110276.

[26] W. Li *et al.*, "A perspective survey on deep transfer learning for fault diagnosis in industrial scenarios: Theories, applications and challenges," *MECHANICAL SYSTEMS AND SIGNAL PROCESSING,* Article vol. 167, 2022 MAR 15 2022, doi: 10.1016/j.ymssp.2021.108487.

[27] X. Wang, B. Yang, Z. Wang, Q. Liu, C. Chen, and X. Guan, "A compressed sensing and CNN-based method for fault diagnosis of photovoltaic inverters in edge computing scenarios," *IET RENEWABLE POWER GENERATION,* Article Early Access 2022, doi: 10.1049/rpg2.12383.

Biographical notes

Xiang-Long You, is currently a PhD candidate at *College of Mechanical and Vehicle Engineering, Chongqing University, China*. He received his Master degree on vehicle engineering from *Beijing Institute of Technology, China*, in 2017. His research interests include fault diagnosis of mechanical systems and power battery systems.
Tel: +86-15937176261; E-mail: xianglongyou@cqu.edu.cn

Zhong-wei Deng, is currently a post doc at *College of Mechanical and Vehicle Engineering, Chongqing University, China.* He received his Ph.D. degree from *Shanghai Jiaotong University, China*, in 2019. His research interests include data-driven and electrochemical mechanism modeling, parameter identification, states estimation, health diagnosis, and cascade utilization of lithium-ion batteries.
E-mail: dengzhongw@cqu.edu.cn

Kai Zhang, is currently a PhD candidate at *College of Automotive Engineering, Chongqing University, China*. His research interests include the fault diagnosis of batteries, sensors, and actuators in lithium-ion battery systems.
E-mail: kaizhang@cqu.edu.cn

Jia-cheng Li, is currently an Engineer at *College of Mechanical and Vehicle Engineering*, *Chongqing University*. His research focuses on hybrid electric vehicles (HEVs), and modeling and thermal management of lithium-ion batteries. He received the B.E. degree in power engineering and the M.S. degree in vehicle engineering from *Chongqing University, Chongqing, China*, in 2014 and 2016, respectively.
E-mail: lijiacheng91@foxmail.com

Hang Yuan, is currently a lecturer at *Henan University of Technology, China*. He received his PhD degree from *Beihang Universtiy, China*, in 2016. His research interests include prognostics and health management, industrial data mining.
E-mail: hangyuan@haut.edu.cn